J Mater Sci (2011) 46:5417–5422
DOI 10.1007/s10853-011-5482-z

# Structural and dielectrical studies on mechano-chemically synthesized indium doped CdS nanopowders

**B. J. Babu · S. Velumani · A. Kassiba**

Received: 3 January 2011 / Accepted: 16 March 2011 / Published online: 29 March 2011


**Abstract** Incorporation of indium (dopant) into CdS crystals have been successfully achieved by a mechanical alloying process. Powders are prepared with various In/Cd ratio from 1 to 10 at% and milled at 300 revolution per minute (rpm) for 60 min. X-ray diffraction (XRD) analysis of milled In doped CdS compound showed that the major phase of the product was wurtzite with grain sizes varying from 37 to 42 nm corresponding to change in In/Cd compositions. High resolution transmission electron microscopy (HRTEM) images as well as Fourier transformation in reciprocal space provide a good pathway to identify the structure of individual CdS nanocrystals, whose dominant phase was determined to be wurtzite structure along with zinc blende structure. Field emission scanning electron microscopy (FESEM) images reveal that CdS crystal prefers to grow along the (001) direction rather than (110) due to its high surface energy. The Raman spectra of CdS:In particles present well-resolved lines at approximately 303 and 600 $cm^{-1}$, corresponding to the first and second-order scatterings, respectively, of the longitudinal optical (LO) phonon mode. Dielectrical studies showed that dielectrical constant ($\varepsilon'$) decreased with increase in frequency, whereas AC conductivity ($\sigma_{AC}$) in In doped CdS increases with increase in frequency and also both the values increased with increase in doping concentration.

**Abbreviations**

| | |
|---|---|
| XRD | X-ray diffraction |
| HRTEM | High resolution transmission electron microscopy |
| FESEM | Field emission scanning electron microscopy |
| EDAX | Energy dispersive analysis of X-rays |
| PLD | Pulsed laser deposition |
| CBD | Chemical bath deposition |
| JCPDS | Joint Committee on Powder Diffraction Standards |
| BDC | Broadband dielectric converter |
| FFT | Fast Fourier transformations |
| IFFT | Inverse fast Fourier transformation |
| LO | Longitudinal optical |

## Introduction

Nanomaterials have drawn interests and attentions due to their special characteristics that differ from that of the bulk solids and molecules. Since nanomaterials possess a large fraction of surface atoms per unit volume due to which these materials will have a huge surface energy and thus, are thermodynamically unstable or metastable [1]. Nanostructured materials especially II–VI semiconductors have recently attracted a lot of attention due to the possibility of their application in optoelectronic devices and photonics. Most II–VI group materials are direct band gap semiconductors (1.7–3.9 eV) with high optical absorption and emission coefficients. Wide band gap CdS (2.4 eV) was

This work was originally presented in Symposium 9 at XIX International Materials Research Congress (IMRC 2010) Cancun, México on 15–19 August 2010.

B. J. Babu · S. Velumani (✉)
Departamento de Ingeniería Eléctrica-SEES, CINVESTAV-IPN, C.P. 07360 Zacatenco, DF, Mexico
e-mail: velu@cinvestav.mx

A. Kassiba
Laboratoire de Physique de l'Etat Condensé—UMR CNRS 6087, Université du Maine, Avenue O. Messiaen, 72085 Le Mans, France

used as a window material in heterojunction solar cells [2]. For high optical throughput with minimal resistive loss, the band gap of window layer should be as high as possible and as thin as possible to maintain low series resistance [3]. The relatively low bandgap of CdS as a window layer reduces blue response, but the effect is mitigated in both CdTe [2, 3] and CIGS [3, 4] devices by utilizing thinner CdS films. Also there are two basic requirements for the window material; (i) low electrical resistivity and (ii) high optical transmittance. Although resistivity and optical transmittance are strongly dependent on preparation conditions, undoped CdS films generally show high electrical resistivity $>10^8$ Ω cm [5]. Thus it is difficult to produce undoped CdS films with low resistivity and high optical transmittance just by controlling the preparation conditions. An effective way to obtain CdS with low resistivity (n-type conductivity) and high optical transmittance is by the creation of excess Cd through various heat treatments [5] and/or incorporation of foreign trivalent donor atoms such as B, Al, Ga and In. Indium is one of the more effective dopant to obtain n-doped CdS because of extra electron coming from the $In^{3+}$ ion placed substitutionally in $Cd^{2+}$ sites. In doped CdS films were prepared by several workers [6–11] using several preparation techniques such as electron beam evaporation [6, 7], hot wall deposition [8], spray pyrolysis [9], pulsed laser deposition (PLD) [10] and chemical bath deposition (CBD) [11]. The chemical spray technique has attracted the attention due to the fact that conductive and transparent In doped CdS thin films can be deposited in a simple and direct way [9]. Before heading towards deposition of In doped CdS films through spray pyrolysis, we have explored on the nano size effect of starting precursors that has been planned to use in the deposition.

In CdS, quantum size effect is observed for crystalline dimensions below 50 Å which is approximately the Bohr exciton diameter in CdS. This ability to tune the band gap of semiconductor to suit any specific application by tailoring the size of the particles has many exciting technological implications. However, in order to optimize the properties, the nanocrystallite sizes should have a narrow distribution in size and shape. Different chemical routes have been followed in the literature to control the shape and their size distribution. These include the uses of surface clipping ligands [12, 13], reverse micellar process [14] and core–shell growth on synthesis of CdS nanoparticles [1]. On the other hand, this paper is focused on study of the properties of In doped CdS nanoparticles synthesized by a simple mechanochemical route using high-energy milling. Application of this processing route in mechanochemistry leads to preparation of various nanosized particles [15]. The differences in the nanoparticle structure and the corresponding properties become critical when the use of mechanochemical methods is applied, consequently the use of new transmission electron microscopy methods have opened the perspectives to understand clearly the variables that influence properties of the solid under study [14]. The chemical bondings (surface reconstruction, heterogeneous composition, dangling bonds) at the interfaces play a key role on the interfacial polarizations between the nanoparticles and hence the electrical and dielectric behaviour of the nanopowders [16]. In these nanosized materials, the relevant data such as the relaxation times and the conductivity are determined and discussed. Although there were few studies on structural aspects of ball milled CdS [17, 18] in the past, to best of our knowledge this is the first attempt to make In doped CdS through mechano-chemical alloying. Decrease in $d$ values drawn from XRD showed that In ions enter substitutionally into Cd sites and presence of indium is clearly observed from the dielectrical studies.

## Experimental details

High purity elemental cadmium sulphide powder (99.9% pure, Sigma-Aldrich) and anhydrous indium trichloride (Sigma-Aldrich) were used as precursor material. Milling of these powders with various In/Cd ratio from 1 to 10 at% was carried out with Retsch planetary ball mill PM 400 at 300 rpm for 60 min, ball-to-powder weight ratio was maintained at 5:1. The effect of In/Cd ratio on both structural and dielectric parameters of CdS nanopowders were studied. The microstructure of milled powders were examined using a Philips X-pert diffractrometer with a CuKα ($\lambda = 1.5406$ Å) radiation. The diffraction angle $2\theta$ was varied from 20° to 80°, and the Miller index ($hkl$) in the obtained diffraction spectra were identified using Joint Committee on Powder Diffraction Standards (JCPDS) card. HRTEM analysis was carried out using FEI Tecnai F30 TEM operating at an accelerating voltage of 300 kV. Surface morphology and composition of the nanopowders were determined using Carl Zeiss Auriga 39-16 accompanied with Bruker energy dispersive analysis of X-rays (EDAX) system. Raman spectra were recorded at room temperature by means of a Raman confocal microspectrometer Horiba Jobin Yvan (Microscopy Olympus BX41) apparatus, using the 632 nm wavelength of a He–Ne Laser. Dielectric measurements were performed over a wide frequency range (0.1 Hz–10 MHz) at room temperature using a Novocontrol broadband dielectric spectrometer [14]. In the given frequency range, a Solartron SI1260 combined with a broadband dielectric converter (BDC) allows impedance and dielectric measurements. With sample cell configuration given elsewhere [15], the sample thickness is determined by the upper electrode used. The thickness and diameter of the upper electrode was 1 and 10 mm, respectively.

## Results and discussion

### Ball milling of In doped CdS

High purity elemental cadmium sulphide and anhydrous indium tri chloride powders were milled using Retsch planetary ball mill PM 400. The colour of the CdS was observed to change from orange through dark yellow to yellow with different indium ratio milling, probably as a result of both work-damage and the reduction of particle size as noticed by Durose et al. [17] and Tsuzuki et al. [18] for milled CdS powders.

### Structural analysis

Figure 1 shows XRD pattern obtained for mechanically alloyed In doped CdS nanoparticles with different In/Cd ratio. All spectra showed polycrystalline hexagonal CdS (JCPDS no. 80-0006) with grain sizes varied from 37 to 42 nm corresponding to change in In/Cd ratio. The average (101) interplanar distance ($d_{101}$) calculated from the XRD patterns for 1, 3, 5, 7 and 10 at% In ratio's are 3.147, 3.146, 3.143, 3.140 and 3.147 Å, respectively. This reduction of $d$ value only can be a consequence of the incorporation of In into the Cd lattice. The smaller ionic radius of $In^{3+}$ (0.94 Å) as compared with that of $Cd^{2+}$ (1.02 Å) can be the cause for the decreasing of $d_{101}$. This can only happen if In ions enter substitutionally in Cd sites. $d_{101}$ in 10 at% In doping is larger than in 7 at%, it is probable the indium impurities originate a lot of disorder in the CdS lattice in such a way that the lattice could be shrunken [11]. No peaks corresponding to indium or indium chloride or indium sulphide were found in the spectra for any In/Cd ratio. Diffraction peaks from (002), (110) and (112) lattice planes in wurtzite structure may be also assigned to the diffraction from (111), (220) and (311) lattice planes in zinc blende structure, both diffraction patterns overlapped together. Therefore, it is difficult to discriminate zinc blende structure from wurtzite in XRD patterns when grain size goes into nanometer scale [19, 20]. However, this structural modification will be confirmed by the HRTEM images in the following section.

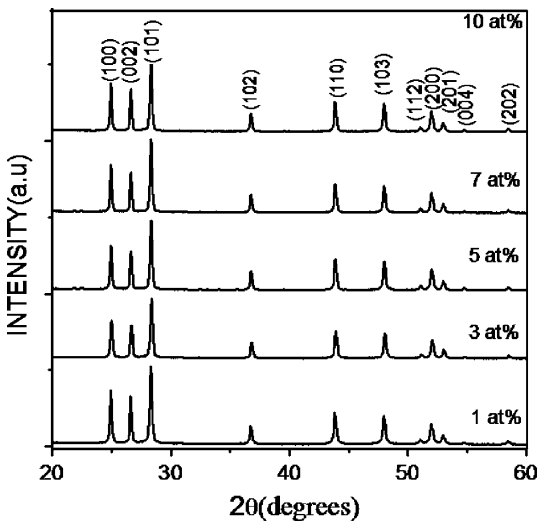


**Fig. 1** X-ray diffraction of mechanical alloying of In doped CdS nanoparticles with various In/Cd ratio

### Microstructure characterization

Due to repeated fracturing and welding process of the particles trapped during collision of ball milling process causes the aggregation of the particles. Nanometer grains are single crystalline while those aggregated big particles are polycrystalline. HRTEM images often give such morphology views of aggregated nanoparticles which are composed of lots of small nanocrystal grains. Figure 2 shows HRTEM image of as-milled In doped CdS nanocrystals. Inserted are their fast Fourier transformations (FFT), inverse fast Fourier transformation (IFFT) images and simulated CdS patterns, from which the particles were identified to be wurtzite structure (particle A) and zinc blende structure (particle B). HRTEM images provide an easy way to identify the structure details of individual nanocrystals by FFT patterns in reciprocal space, thus distinction between the wurtzite structure and zinc blende structure in as-milled CdS particles becomes much easier.

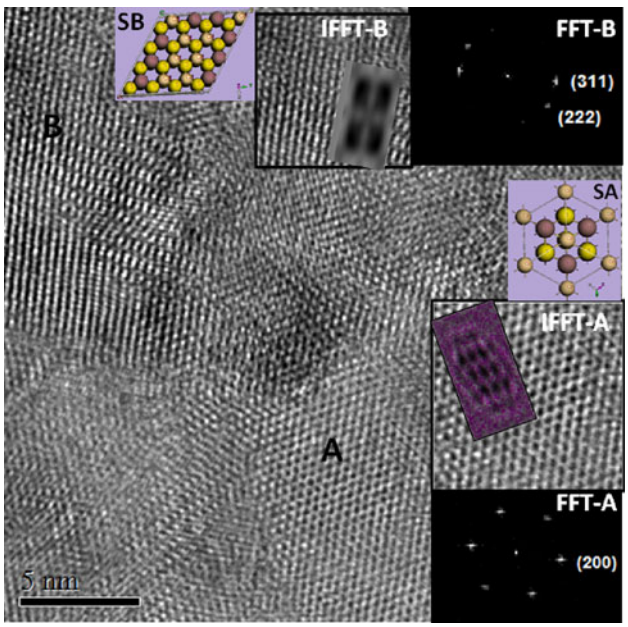


**Fig. 2** HRTEM images of the as-milled CdS nanoparticles doped with 5 at% of indium, showing the mixture phase of hexagonal and cubic structures

Figure 2 shows several CdS nanoparticles aggregate together where particle A is assigned to be the wurtzite structure exhibiting lattice plane (200) with $d$ spacing of 1.768 Å and particle B is identified to be the zinc blende structure exhibiting lattice planes (311) and (222) with $d$ spacing of 1.64 and 1.57 Å, respectively. The other particles are serious aggregated and hard to distinguish each other. It is very difficult to draw out these classifications from XRD patterns in Fig. 1, but HRTEM images did it. The phase transition may be induced by high pressure impacting on the powders from the ball against the wall during the high frequency rotation movement of the vial [19]. A similar conclusion has drawn out for CdSe [19] and CdS [20] nanoparticles synthesized using mechanical alloying process by Tan et al. It is well known that when hexagonal CdS or CdSe powder is subjected to grinding or milling, substantial changes in structure occur. Progressive change from the expected hexagonal to a more cubic-like structure due to mechanical alloying is observed by many others [17–21]. In Fig. 2, SA and SB are simulated hexagonal and cubic structures, respectively. Inserted IFFT-A and IFFT-B images are matched with simulated HRTEM images generated using SA and SB structures. Simulated patterns of hexagonal and cubic structures are fitted well with experimental patterns confirming the particles A and B are hexagonal and cubic structures, respectively.

## Surface morphology and compositional analysis

From high resolution scanning electron microscopy (HRSEM) micromorphology of the as-milled In doped CdS nanopowders were analyzed. Figure 3 shows HRSEM images of undoped, unmilled and In doped as-milled CdS nanopowders. It can be seen that the product mainly consists of hexagon like structures, which agrees with XRD pattern. Particle size between 51.76 and 139.4 nm was observed which is comparable with average grain size obtained from XRD. Milling of powder precursor influenced particle size and In doping. Elongated growth along the (001) direction of rod-like crystals is favoured. Some rods emerge on the side surface, which are symmetrically separated between each other and initially grow along the (110) direction. CdS crystal prefers to grow along the (001) direction rather than the (110) due to its high surface energy [22]. From Table 1, it is evident that doping of Indium into cadmium sites saturates at 7 at% of indium since the quantity of indium detected in 10 at% is less compared to 7 at%. From Fig. 3f, we can notice that excess of indium trichloride are present in the powders after milling indicating that indium impurities not totally replaced in substitutional and interstitial sites of cadmium which may be due to solubility limit [11].

**Table 1** Elemental composition of In doped CdS nanopowders

| Percentage of indium doped | Cd (at%) | S (at%) | In (at%) |
|---|---|---|---|
| 0 | 52.98 | 47.02 | – |
| 1 | 52.82 | 46.88 | 0.29 |
| 3 | 51.80 | 47.56 | 0.64 |
| 5 | 52.88 | 44.52 | 2.60 |
| 7 | 56.20 | 38.88 | 4.92 |
| 10 | 51.68 | 46.01 | 2.31 |

## Raman spectra

The Raman spectra of the CdS:In nanoparticles given in Fig. 4 present a well-resolved line at approximately 303 $cm^{-1}$, corresponding to the first order scattering of the longitudinal optical (LO) phonon mode [10, 11]. The second-order scattering of LO phonons is also visible at approximately 600 $cm^{-1}$, similar trend has been observed by Perna et al. [10] for In doped CdS films prepared by PLD. As shown, the peak at 303 $cm^{-1}$ is asymmetric; suggesting a superposition of more than one mode. This peak consists of a superposition of three different peaks; the cubic 1LO or hexagonal A1(LO)/E1(LO) peak. Raman spectra present well defined LO peaks, which broaden in higher doped samples, due to the increase of compositional disorder. In addition, a shoulder appears at approximately 344 and 365 $cm^{-1}$, it can be due to disorder activated combination modes or local modes involving indium [10].

## Dielectrical studies

Figures 5 and 6 show frequency spectra of dielectrical constant ($\varepsilon'$) and AC conductivity ($\sigma$) of In doped CdS nanoparticles, respectively. From Fig. 5 it is clear that, with increase in indium doping value dielectrical constant increased except for 10 at% and decreased with increase in frequency [23]. The nature of dielectric permittivity related to free dipoles oscillating in an alternating field. (i) At very low frequencies ($\omega \ll 1/\tau$, $\tau$ is the relaxation time), dipoles follow the field and $\varepsilon' \approx \varepsilon_s$ (value of the dielectric constant at quasi-static field). (ii) With increase in frequency ($\omega < 1/\tau$), dipoles begin to lag behind the field and $\varepsilon'$ slightly decreases. (iii) When frequency reaches the characteristic frequency ($\omega = 1/\tau$), the dielectric constant drops (relaxation process) and (iv) At very high frequencies ($\omega \gg 1/\tau$), dipoles can no longer follow the field and $\varepsilon' \approx \varepsilon_\infty$ [24, 25]. Since dielectrical constant is directly related to capacitance, the curves related capacitance (not shown here) also showed similar trend.

The conductivity can be expressed as $\sigma(\omega) = \omega\varepsilon_0\varepsilon''$. Here $\sigma$ is the real part of the conductivity and $\varepsilon''$ is the imaginary part of dielectric constant. It is seen from Fig. 6

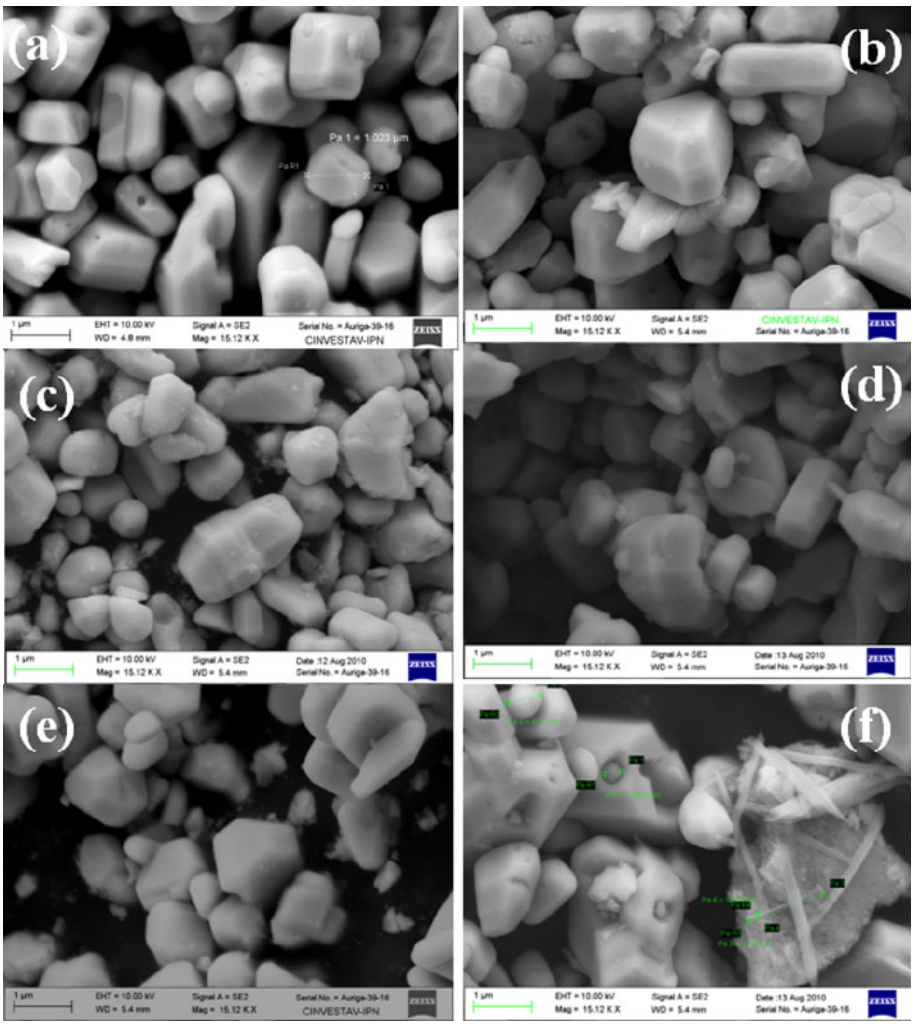


**Fig. 3** HRSEM images of **a** undoped and unmilled CdS powder, **b** 1 at%, **c** 3 at%, **d** 5 at%, **e** 7 at% and **f** 10 at% In doped milled CdS powders

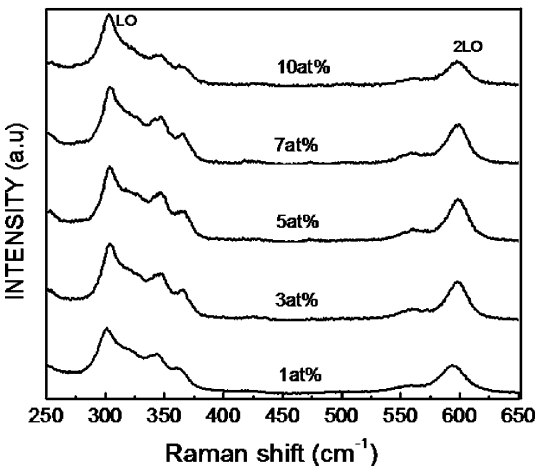


**Fig. 4** Raman spectra of mechanical alloying of In doped CdS nanoparticles with different In/Cd ratio

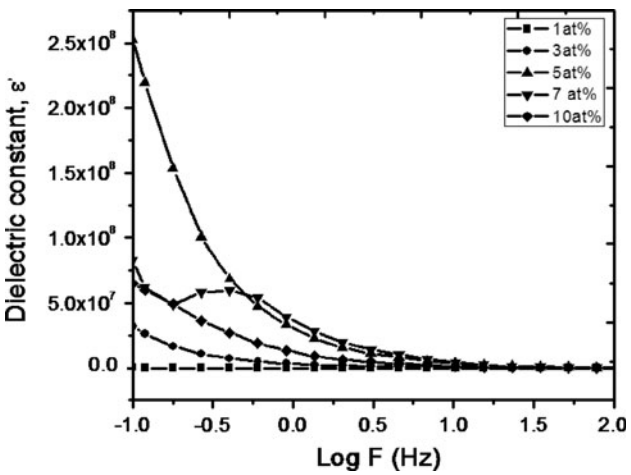


**Fig. 5** Dielectric constant of In doped CdS nanoparticles

that $\sigma$ decreases with decreasing frequency and becomes independent of frequency after a certain value [24]. Extrapolation of this part towards lower frequency will give $\sigma_{DC}$. AC conductivity ($\sigma_{AC}$) in CdS increases with increase in frequency. The real parts of conductivity spectra can be explained by the power law defined as

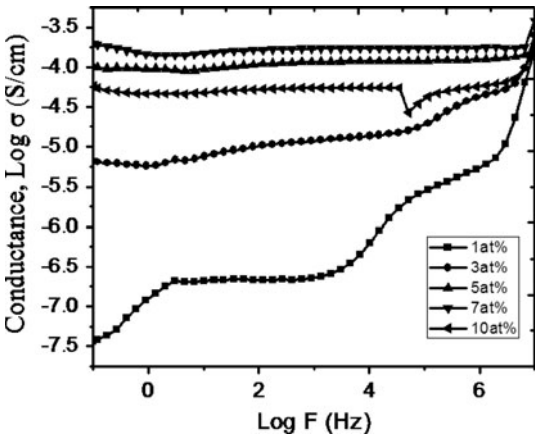


**Fig. 6** AC conductivity of In doped CdS nanoparticles

$$\sigma = \sigma_{DC}\left[1 + \left(\frac{\omega}{\omega_H}\right)^n\right] \quad (1)$$

where $\sigma_{DC}$ is the DC conductivity, $\omega_H$ is the hopping frequency of the charge carriers and n is the dimensionless frequency exponent. Also from Fig. 6 it can be seen that, $\sigma$ increases with increase in In doping except for 10 at%. It is evident from XRD and HRSEM analysis that, the indium doping for 10 at% is less than other samples and therefore carrier concentration in turn conductivity of 10 at% In doped CdS is low. During dielectrical measurements at higher temperatures, the samples started melting because minor quantity of indium trichloride was present in the sample. So we were not able to proceed for further studies on samples at higher temperatures.

## Conclusions

In doped CdS nanoparticles are prepared by fast, simple and safe method using ball milling. Further milling time is required to observe quantum confinement of the CdS nanoparticles. XRD showed polycrystalline hexagonal phase of In doped CdS. However, Raman, HRTEM showed presence of cubic phase also. FESEM images revealed excess of indium trichloride at higher doping values. EDAX analysis showed presence of indium in the powders. AC conductivity ($\sigma_{AC}$) in CdS increases with increase in frequency and also with increase in doping concentration except for higher doping values. For all the powders the dielectric constant are observed to reach saturation at high frequencies. We conclude that 5 at% doping of indium will be yielding better results and future work will be carried out with higher milling time at 5 at%.

**Acknowledgements** Authors thank Dr. Miguel Avalos of IPICyT for providing HRTEM facilities and Miguel Galvan of SEES-IE, CINVESTAV for Raman measurements. We are thankful to N. Errien of Université du Maine, France for dielectrical measurements. B. J. Babu thanks CONACyT for providing scholarship to pursue doctoral program in Mexico.

## References

1. Cao G (2004) Nanostructures and nanomaterials synthesis, properties and applications. Imperial College Press, London
2. Afzaal M, O'Brien P (2006) J Mater Chem 16:1597
3. Chopra KL, Paulson PD, Dutta V (2004) Prog Photovolt Res Appl 12:69
4. Shi CY, Sun Y, He Q, Li FY, Zhao JC (2009) Sol Energy Mater Sol Cells 93:654
5. Cha D, Kim S, Huang NK (2004) Mater Sci Eng B106:63
6. Megahid NM, Wakkad MM, Shokr EKH, Abass NM (2004) Phys B 353:150
7. Bertran E, Morenza JL, Esteve J, Codina JM (1984) J Phys D Appl Phys 1(7):1679
8. Dhere NG, Moutinho HR, Dhere RG (1987) J Vac Sci Technol A 5(4):1956
9. Ikhmayies SJ, Ahmad-Bitar RN (2008) Amc J Appl Sci 5(9):1141
10. Perna G, Capozzi V, Ambrico M, Augelli V, Ligonzo T, Minafra A, Schiavulli L, Pallara M (2004) Thin Solid Films 453–454:187
11. Dávila-Pintle JA, Lozada-Morales R, Palomino-Merino R, Rebollo-plata B, Martinez-Hipati C, Portillo-Moreno O, Jimenez-Sandoval S, Zelaya-Angel O (2006) AZojomo (ISSN 1833-122X) 2:1
12. Tiwari S, Tiwari S (2006) Cryst Res Technol 41(1):78
13. Kotkata MF, Masoud AE, Mohamed MB, Mahmoud EA (2009) Phys E 41:1457
14. Pinna N, Weiss K, Sack-kongehi H, Vogel W, Urban J, Pileni MP (2001) Langmuir 17:7982
15. Godočíková E, Balaz P, Gock E, Choi WS, Kim BS (2006) Powder Technol 164:147
16. Tabellout M, Kassiba A, Tkaczyk S, Laskowski L, Swiatek J (2006) J Phys Condens Matter 18:1143
17. Durose K, Fellows AT, Brinkman AW, Russell GJ, Woods J (1985) J Mater Sci 20:3783. doi:10.1007/BF01113788
18. Tsuzuki T, McCormick PG (1997) Appl Phys A 65:607
19. Tan GL, Du JH, Zhang QJ (2009) J Alloys Compd 468:421
20. Tan GL, Zhang L, Yu Xue-Feng (2010) J Phys Chem C 114:290
21. Dutkova E, Balaz P, Pourghahramani P, Velumani S, Ascencio JA, Kostova NG (2009) J Nanosci Nanotechnol 9:1
22. Xue M, Zhang X, Wang X, Tang B (2010) Mater Lett 64:1357
23. Velumani S, Narayandass SaK, Mangalaraj D, Sebastian PJ, Mathew X (2004) Sol Energy Mater Sol Cells 81:323
24. Tripathi R, Kumar A, Sinha TP (2009) Pramana J Phys 72(6):969
25. Matheswaran P, Sathyamoorthy R, Saravanakumar R, Velumani S (2010) Mater Sci Eng B 174:269